Faraday Discussions
Cite this: *Faraday Discuss.*, 2023, **246**, 141

PAPER

Logic gating of low-abundance molecules using polyelectrolyte-based diodes†

Barak Sabbagh, [a] Zhenyu Zhang [bc] and Gilad Yossifon *[ac]

Received 6th March 2023, Accepted 20th March 2023
DOI: 10.1039/d3fd00061c

Bioinspired artificial ionic components are extensively utilized to mimic biological systems, as the vast majority of biological signaling is mediated by ions and molecules. Particular attention is given to nanoscale fluidic components where the ion transport can be regulated by the induced ion permselectivity. As a step from fundamentals toward ion-controlled devices, this study presents the use of ionic diodes made of oppositely charged polyelectrolytes, as a gate for low-abundance molecules. The use of ionic diodes that exhibited nonlinear current–voltage responses enabled realization of a basic Boolean operation of an ionic OR logic gate. Aside from the electrical response, the asymmetric ion transport through the diode was shown to affect the transport of low-abundance molecules across the diode, only allowing crossing when the diode was forward-biased. Integration of multiple diodes enabled implementation of an OR logic operation on both the voltage and the molecule transport, while obtaining electrical and optical output readouts that were associated with low and high logic levels. Similarly to electronics, implementation of logic gates opens up new functionalities of on-chip ionic computation *via* integrated circuits consisting of multiple basic logic gates.

Introduction

Complex ionic regulation in aqueous solutions is ubiquitous in natural systems, as the vast majority of biological signaling is mediated by ions and molecules rather than electrons. For example, cells and neurons polarize and depolarize as a result of the transport of ionic charge carriers across the cell membrane *via* ion channels.[1] Artificially designed ionic components and circuits that generate, transmit, and store signals based on ion transport provide a means of effectively mimicking biological communication and computation. This emerging discipline is known as "iontronics".[2–4] Iontronics can be applied for various practical applications that work in an aqueous environment and rely on increasingly sophisticated control over ion and molecule transport, including ionic circuits for

[a]*Faculty of Mechanical Engineering, Technion – Israel Institute of Technology, Israel*
[b]*School of Mechanical Engineering, Southeast University, China*
[c]*School of Mechanical Engineering, Tel-Aviv University, Israel. E-mail: gyossifon@tauex.tau.ac.il*
† Electronic supplementary information (ESI) available. See DOI: https://doi.org/10.1039/d3fd00061c

sensing,[5,6] information processing,[7] and drug delivery.[2] Iontronic devices often consist of functional nanoscale components integrated within a microfluidic system. These nanofluidic components have been attracting considerable attention both at the fundamental physical level and in promising applications beyond biomimetic information processing, including chemical and biochemical sensing,[8,9] energy harvesting,[10,11] single-molecule detection,[12,13] and electrokinetic preconcentration.[14,15] In nanoscale systems, such as nanochannels and nanoporous membranes, ion transport can be regulated by the inherent functional surface groups and their associated charge density. Interfacial electric double layers (EDLs), with a characteristic length termed the Debye length (typically 1–100 nm), are spontaneously formed to screen the surface charge.[16] When the Debye length is comparable to the nanoscale dimension (*e.g.*, height or width) of the nanofluidic component, the EDLs with opposite surfaces overlap and induce ion permselectivity.[17] This symmetry-breaking effect prevents transport of the coions (*e.g.*, anions for the negatively charged surface) through the ion-permselective medium due to electrostatic repulsion, while promoting transport of the counterions (*e.g.*, cations for the negatively charged surface). In an aqueous electrolyte solution consisting of dissolved salts (*e.g.*, KCl or NaCl) and charged low-abundance molecules, the latter act as third species, *i.e.*, they only respond to the electric field-related effects and have a negligible effect on the local ionic conductivity. Electrophoretically driven transport of low-abundance charged molecules through the permselective structure is affected by the type and concentration of the dissolved solutes, the nanostructure and surface properties, and the molecule properties, including size, charge, and surface interaction.[18–21]

Of the various techniques available for realizing ionic permselective structures, polyelectrolyte gels[22–24] are relatively simple to handle and have been extensively used. Polyelectrolytes are water-swollen porous polymer networks with ionized groups in the repeating monomeric units. They are synthesized by the polymerization of ionic liquid monomers, and their hydrophobicity is a distinctive feature that renders them stable in water.[25] In order to maintain charge neutrality, the ionized groups attract mobile ions of the opposite charge (counter-ions) within the water-swollen pores. Hence, they can be categorized as cation- (CEP), anion- (AEP), or zwitterion-exchange polyelectrolytes (ZEP), depending on their backbone groups. Numerous realizations of iontronic diodes using polyelectrolytes have been reported in the past decade.[26–32] A polyelectrolyte diode is comprised of two interfacing oppositely charged homogenous polyelectrolytes. The permselectivity-driven asymmetric ion transport through the bipolar structure exhibits a nonlinear current–voltage (I–V) response on application of an external electric field, with high conductance in the forward-biased electric field direction and low conductance in the reverse-biased direction. This non-linear response is predominantly controlled by the ion concentration at the junction between the two polyelectrolytes (with permselectivity to oppositely charged ions) and is similar, in terms of apparent I–V, to that of a silicon-based p–n junction diode. And yet, due to the non-ideal ion permselectivities, as described in the Teorell–Meyer–Sievers theory,[33,34] a minority of co-ions can still cross the bipolar polyelectrolyte layers from side to side (termed crossover). Besides the ion permselectivity, the crossover is expected to be impacted by the valence, pH, and pK_a of the electrolyte ions and molecules.[35] Considering convective transport effects due to electroosmotic flow (EOF), the opposite surface charges of the polyelectrolytes

that form the bipolar diode generate EOF in opposite directions, resulting in approximately zero net flow.[36,37] Furthermore, crossover due to pressure-driven convective transport is considered to be negligible compared to electromigration due to the extremely low hydrodynamic permeability of the nanoporous polyelectrolytes.[18] Previous studies on iontronic circuits have shown that multiple ionic diodes can be integrated within a microfluidic device to perform basic logical functions, such as OR and AND logic gates, on the electrical signal.[26,38–41] However, most of the reported logical operations considered only the overall ionic electrical current and potential, which were independent of the ionic species type, and completely neglected the transport of low-abundance species.

This work investigated the crossover of low-abundance molecules in a polyelectrolyte bipolar diode within a microfluidic device (Fig. 1a). This extends previous studies that mainly focused on the transport of the electrolyte's background ionic species, which dominate the electrical response. We showed that the diode acts as a molecular gate that allows the passage of low-abundance molecules only under certain conditions. Polyelectrolyte regions spotted on the microfluidic channel (external to the diode) were used to adsorb the molecules that crossed the diode, resulting in a localized increase in their concentration. These polyelectrolyte spots were utilized as a logical indicator of the presence of target fluorescently labeled molecules, with bright and dark spots equivalent to logic levels '1' and '0', respectively. The proposed functionality of the diode as a molecular gate was extended to integrated ionic circuits consisting of multiple bipolar diodes and interconnecting microchannels that form a Boolean function of an OR logic gate. The logical disjunction was implemented for both the electrical signal and the molecular gating, as they were proven to be coupled together.

Materials and methods

Fabrication of a polyelectrolyte-based ionic diode within a microfluidic device

Two glass slides were used as substrates for the microfluidic chip. The slides were cleaned (piranha solution, $H_2SO_4 : H_2O_2 = 3 : 1$, for 10 min), drilled (Dremel 4000 with a diamond grinding bit, $\varnothing = 1.8$ mm, Proxxon) with multiple holes, and treated with a methanol solution containing 0.5% 3-(trimethoxysilyl)propyl methacrylate (TMSMA, Sigma) and 0.5% acetic acid, for 2 h, to ensure a covalent link between the substrate and the polyelectrolyte. A 25 μm-thick double-sided adhesive (3M™ Optically Clear Adhesive 8146-1-ND) was patterned (CAMEO silhouette 4) and sandwiched between the two glass slides, thereby forming the microfluidic channels. The anionic and cationic polyelectrolytes were synthesized and immobilized by UV polymerization (100 mJ cm^{-1} and 200 mJ cm^{-1}, respectively) of 4.2 M diallyldimethylammonium chloride (DADMAC, Sigma) and 2-acrylamido-2-methyl-1-propane sulfonic acid (AMPSA, Sigma), respectively, in the presence of a photo-initiator (2%, 2-hydroxy-4′-(2-hydroxyethoxy)-2-methylpropiophenone, Sigma) and crosslinker (2%, *N*,*N*′-methylenebis(acrylamide), Sigma). To form a bipolar diode, only half of the diode region was left uncovered during the polymerization process for each polyelectrolyte, later resulting in immobilization of the two oppositely interfacing charged polyelectrolytes. The entire procedure closely followed previously reported works.[42] The polyelectrolyte indicator spots were similarly synthesized after forming the diodes, wherein each spot contained only a single type of polyelectrolyte, tailored

to accommodate the net charge of the target molecule that needed to be adsorbed and visualized. A bright-field microscopy image of the interface formed between the two oppositely charged polyelectrolytes can be seen in Fig. S1.†

Electrical and optical measurements

A 10 mM KCl electrolyte ($\sim$1.7 mS cm^{-1}) was used in all experiments. For the electrical measurements, a sourcemeter (Keithley 2636) and silver–silver chloride electrodes (Ag–AgCl, A-M Systems, 0.015″ diameter) immersed in the electrolyte within designated locations were used to apply and measure the electrical potential/current. *I–V* curves were obtained by sweeping the voltage from reverse-(-1 V) to forward-bias (+1 V), at a scan rate of +1.6 mV s^{-1}, while measuring the current. Before the *I–V* measurement, the diode was subjected to -1 V for 300 s to reach its steady-state reverse-bias condition. The diode's rectification ratio was evaluated *via* its chronoamperometric response (*i.e.* measuring the current following a step-wise application of a constant voltage of $\pm$1 V) after 300 s. The diode logic gate (DLG) inputs were activated or deactivated by biasing with either +1 V or 0 V, respectively. Open-circuit potential (employing high impedance for no-current conditions) measurements were used as the circuit's electrical output readouts. For the optical measurements, the microfluidic device was visualized and captured using a spinning disc confocal system (Yokogawa CSU-X1), and an inverted microscope (Eclipse Ti-U, Nikon) equipped with an electron-multiplying charge-coupled device (EMCCD) and camera (Andor iXon3). Low concentrations, relative to the background ionic electrolyte concentrations, of fluorescently tagged anionic (Alexa Fluor 488, Thermo Scientific Inc.) and cationic (Atto Rho6G and ATTO 465, Sigma) dyes were used as the low-abundance molecules. The fluorescence intensity of each dye molecule was individually captured by varying the monochromatic laser source and the filter based on the excitation/emission wavelength of the dye (Fig. S2†). The local fluorescence intensity was normalized (AU units) to the background intensity outside the microfluidic channels.

Numerical simulations

The simplified numerical model of the experimental setup consisted of a four-layer system with a two-dimensional geometry in which two microchannels (each 5*L*-long) were connected by a pair of oppositely charged ionic permselective media that represented the polyelectrolytes (each *L*-long), which together represented the diode (Fig. 2a). The fully coupled Poisson (eqn (1)) and Nernst–Planck (eqn (2)) equations, satisfying the continuity of ionic fluxes (eqn (3)), were solved (COMSOL Multiphysics 5.3) under the assumption of the absence of chemical reactions or convection within the system. A mixture of a symmetric binary ($Z_\pm = \pm 1$) electrolyte of equal ion diffusivities ($D = D_\pm$) and monovalent ($Z_\pm^A = \pm 1$) low-concentration analytes ($C_\pm^A$, 3 orders of magnitude lower relative to the background ionic electrolyte concentrations $C_\pm$ of the dissolved salts) was simulated. Subscripts + and $-$ represent positive and negative charges, respectively. The superscript A represents the analyte, while the absence of the superscript represents the electrolyte ions.

$$\nabla^2 \Phi = -\frac{\rho_e}{\varepsilon_0 \varepsilon_r} \quad (1)$$

$$j_k = -D_k\left(\nabla C_k + \frac{F}{RT}Z_k C_k \nabla \Phi\right) \tag{2}$$

$$\frac{\partial C_k}{\partial t} + \nabla \cdot j_k = 0 \tag{3}$$

where Φ is the electric potential, ε_0 and ε_r are the permittivity of a vacuum and the relative permittivity of the electrolyte, respectively, t is the time, j_k is the ionic flux density, F is the Faraday constant, R is the universal gas constant, and T is the absolute temperature. The subscript k stands for the different electrolyte and analyte species. Assuming a fixed volumetric charge density, N, representing the polyelectrolytes' ionized surface groups as in the classical models of permselective membranes,[43,44] the ionic charge density ρ_e can be written as follows for the microchannel (eqn (4)) and polyelectrolyte (eqn (5)) regions:

$$\rho_e = F\sum_k Z_k C_k \tag{4}$$

$$\rho_e = F\left(\sum_k Z_k C_k \pm N\right) \tag{5}$$

where positive and negative values of N stand for AEP and CEP, respectively. The electric current density, i, was calculated as follows:

$$i \equiv F\sum_k Z_k j_k \tag{6}$$

The following normalizations were used to present the results: ion concentration $C_k = C_{k,0}\tilde{C}_k$, electrical potential $\Phi = (RT/F)\tilde{\Phi}$, ionic flux density $j_k = (DC_{+,0}/L)\tilde{j}_k$, current flux density $i = (FDC_{+,0}/L)\tilde{i}$, and time $t = (L^2/D)\tilde{t}$. Here, the tilde notations denote nondimensional parameters. $C_{k,0}$ denotes the initial concentration of species k at $t = 0$. As an initial condition, only the electrolyte was presented in the system ($\tilde{C}_{\pm,0} = 1$, $\tilde{C}^{A}_{\pm,0} = 0$). The analyte concentrations and the electric potentials at the inlet and outlet boundaries were separately set for each experiment.

Results and discussion

Electrical and optical characterization of the diode

The non-linear behavior of the diode was apparent in the I–V (current–voltage) curve (Fig. 1b). When forward-biasing the diode ($0 < V < +1$ V), the measured current increased sharply, with an average slope of 420 pA $(\text{mV})^{-1}$, reaching a forward current of $I_F = 4.2 \times 10^{-1}$ μA at $V = +1$ V. In this state, the diode was considered open. In contrast, reverse-biasing resulted in a moderate current that barely changed with the voltage (16 pA $(\text{mV})^{-1}$) and saturated to a value of reverse current $I_R = -1.6 \times 10^{-2}$ μA at $V = -1$ V, in which the diode was considered closed. The rectification ratio, RR, defined as the ratio of these currents in opposite polarity ($|I_F/I_R|$), was ~25. The higher the RR, the more precise the control over the ion flux and the corresponding electrical response of the diode. The fluorescence intensity of the anionic dye (Alexa Fluor 488) was used as an indicator for the dynamic changes

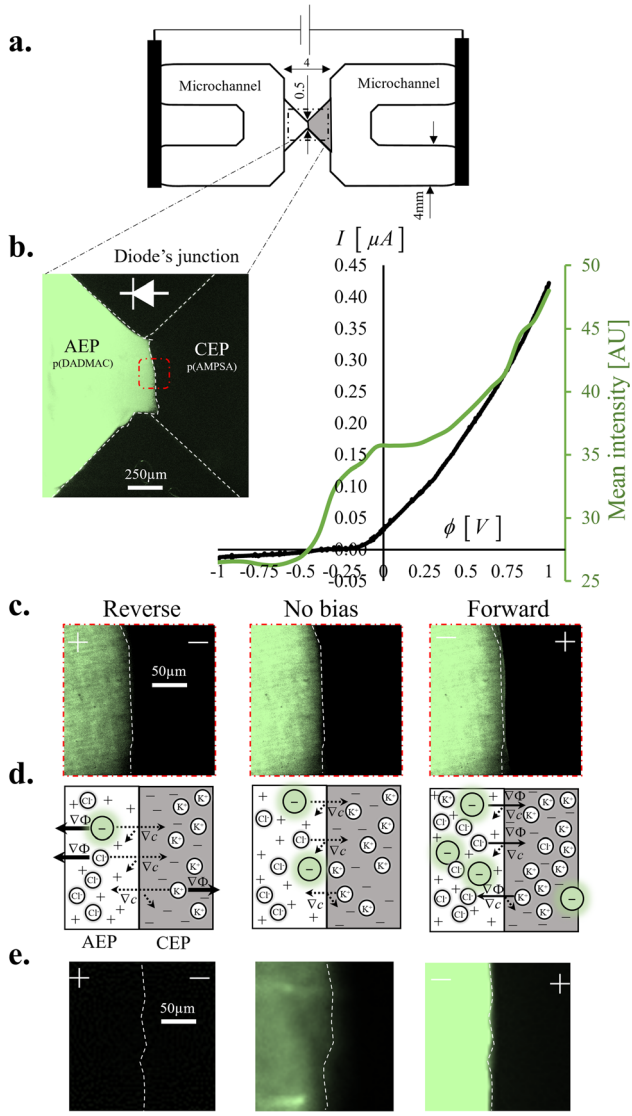

Fig. 1 Characteristic response of the diode: experimental observations. (a) Schematic of the experimental system comprised of two wide (4 mm) microchannels connected by a narrow junction (minimum width of 0.5 mm) interfacing anion-exchange and cation-exchange polyelectrolytes (AEP and CEP, respectively). (b) Left: fluorescence image after stabilization of the diode junction following the introduction of a mixture of an electrolyte (10 mM KCl) and anionic fluorescent dye (1 μM Alexa Fluor 488) into the microchannels. Right: experimentally measured current–voltage (I–V) curve (solid black line) and the corresponding average measured fluorescence intensity (solid green line in AU units) at the interface (red dashed square). The voltage sweeping (+1.6 mV s^{-1}) direction was set from reverse (−1 V) to forward bias (1 V). (c) Zoomed-in fluorescence images of the junction (red dashed square in b), taken during the I–V sweep (at times t = 0, 600 and 1200 s corresponding to −1, 0 and +1 V). (d) Schematics of the ion transport mechanisms near the AEP–CEP interface, including diffusion (∇c) and electromigration ($\nabla\phi$) of ions. The arrows indicate the flux directions, while solid/dashed lines represent a major/minor flux. The electrolyte ions (Cl^- and K^+) and the anionic fluorescent dye are represented by white and green circles, respectively. (e) Zoomed-in fluorescent images of the interface (similar to (c)), taken after 12 h of constant electric potential activations (−1, 0, +1 V).

of the dye concentration within the AEP at different applied potentials, ϕ. The dye exhibited a third-species behavior, with a negligible effect on the electric field, electric current, and space charge due to its significantly lower concentration ($C_-^A = 10\ \mu M$) compared to that of the dissolved electrolyte salt ion ($C_\pm = 10$ mM). As a result, changes in the dye concentration did not necessarily mirror the changes exhibited by the electrolyte ions. The intensity of the anionic dye within the AEP region gradually increased with the transition from reverse bias (−1 V) to no bias (0 V) and up to forward bias (+1 V) (Fig. 1c). This corresponded with a transition from electrolyte ion depletion to enrichment at the diode junction (Fig. 1d). Longer operation times of several hours (12 h) at these continuously applied potentials resulted in enhanced changes in the intensity from an almost complete depletion of the dye (−1 V) to a strong enrichment (+1 V), while the low intensity in the CEP region remained almost unchanged (Fig. 1e).

Interestingly, some of the dye molecules that reached the AEP–CEP interface overcame the electrostatic barrier and succeeded in crossing the diode junction. Such crossover is only possible in the case of non-ideal ionic permselectivity; in the case of ideal selectivity, the obstruction is absolute. The coupled Poisson (eqn (1)), Nernst–Planck (eqn (2)) and continuity (eqn (3)) equations provided a numerical solution of the ionic transport across the bipolar diode. There are several possible mechanisms controlling ionic transport across the diode (eqn

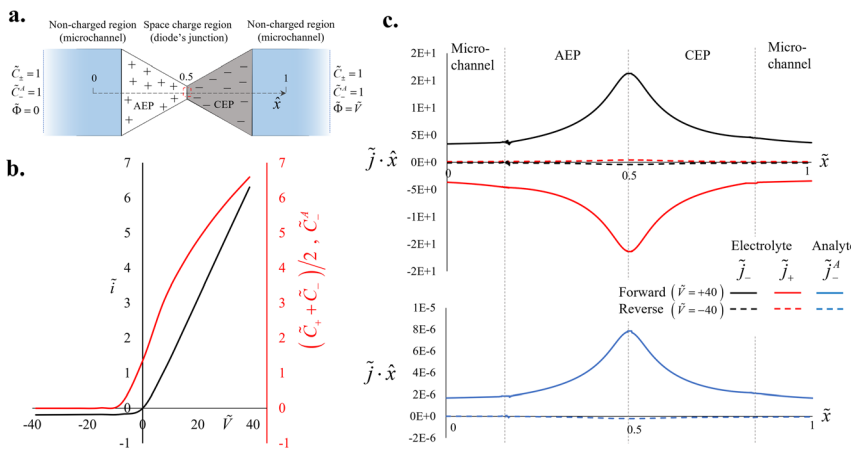

Fig. 2 Numerical investigation of the bipolar diode response. (a) Schematic of the numerical model consisting of two non-charged microchannel regions (blue), and an effective charged region (the diode) composed of anion- and cation-exchange polyelectrolytes (AEP and CEP, marked in white and grey, respectively). The coordinate system ($\tilde{x}$) and boundary conditions of the potential ($\tilde{\Phi}$), electrolyte concentration ($\tilde{C}_\pm$) and anionic dye concentration (the analyte, $\tilde{C}_-^A$) are presented for clarity. (b) Numerically calculated current–voltage ($\tilde{i}$–$\tilde{V}$) curve (black line) with a diode rectification ratio of RR = 34 at $\tilde{V} = 40$. The red line represents the electrolyte salt ($(\tilde{C}_+ + \tilde{C}_-)/2$) and analyte $\tilde{C}_-^A$ concentrations at the interface region between the two polyelectrolytes ($\tilde{x} = 0.5$). (c) Flux density distributions along the $\tilde{x}$ axis. $\tilde{j}_+$ and $\tilde{j}_-$, represent the cation (red) and anion (black) electrolyte flux densities, respectively (top plot). $\tilde{j}_-^A$ represents the analyte flux density (blue) (bottom plot). Each flux was plotted for the reverse- (dashed line) and forward-biased (solid-line) diode state. The spatial distribution of the normalized space change density ($\tilde{\rho}_e$) and the ion concentrations can be seen in Fig. S3.†

(3)), including water splitting/dissociation,[45,46] recombination reactions,[47] temporal variation of the ion concentrations due to concentration–polarization effects,[28,48] and ion crossover.[28,35] The lack of an interfacial catalytic layer between the two polyelectrolytes and the relatively low applied potentials (<|1| V) significantly reduced the probability of water dissociation into protons (H^+) and hydroxide ions (OH^-), and the reverse process of recombination of ions into water molecules.[47] Elongated operation times ($>L^2/D$) of constant electric potentials resulted in stabilization of the system and of the induced concentration gradients, which along with the deviation from ideal-permselectivity conditions enabled ion crossover that contributed to the steady-state current. The transport of ions across the polyelectrolytes was confirmed by numerical simulations of a simplified 2D model of the diode (Fig. 2). As observed experimentally, the model showed that the conductance (Fig. 2b), *i.e.*, the slope of the $\tilde{i}$–$\tilde{V}$ curve describing the quasi-steady-state response, increased as the potential increased from negative to positive values, leading to a rectification ratio of the current $RR = \tilde{i}_F/\tilde{i}_R = 34$ at $\tilde{V} = \pm 40$. At any point along the junction region ($0 < \tilde{x} = x/3L < 1$), the forward-flux densities of the electrolyte cations ($\tilde{j}_+$) and anions ($\tilde{j}_-$) were consistently ~34-times higher than the reverse-flux densities (Fig. 2c). Narrowing the width of the diode junction caused an increase in the absolute value of the ion-flux density (having a maximum value at $\tilde{x} = 0.5$); nevertheless, the rectification ratio was preserved under steady-state conditions. The anionic analyte exhibited similar behavior, although the obtained fluxes ($\tilde{j}_-^A$) were much lower compared to the ionic electrolyte fluxes due to the low concentration of the analyte. Thus, the higher the RR, the more effective the regulation of the analyte flux crossing the diode.

Single-diode gating of low-abundance molecules

The regulation of ion crossover through the diode was utilized to gate charged low-abundance molecules (Fig. 3). To observe molecule transport from one side of the diode to the other side, anionic (Alexa Fluor 488) and cationic (Atto Rho6G) dyes were used as the target molecules. The low-concentration dyes were separately introduced to either the anodic or cathodic side only, while the diode was subjected to different activation modes, *e.g.*, reverse, forward, and no bias (−1, 1 and 0 V, respectively). Measurement of fluorescence at the opposite side (where initially no dye was introduced) indicated that the dye molecules successfully crossed the diode. The number of molecules that crossed the diode was in correlation with the intensity of the fluorescence signal, which increased over time as more molecules crossed the junction. Thereby, operation for a long period of time (overnight operation of up to 15 hours) was necessary to reach above their limit of detection concentration value. Molecules that crossed the diode diffused towards the reservoir and were also subjected to 'ion concentration-polarization' at the polyelectrolyte–microchannel interfaces,[42,48] which both affected the observed intensity. To overcome these effects, polyelectrolyte spots (~0.5 mm-diameter circles) external to the diode were used to adsorb molecules that successfully crossed the diode, thereby creating a local area with a higher fluorescence intensity due to their accumulation. Anionic molecules were spontaneously adsorbed onto the AEP, while the cationic molecules were adsorbed onto the CEP. These experiments demonstrated that a positive

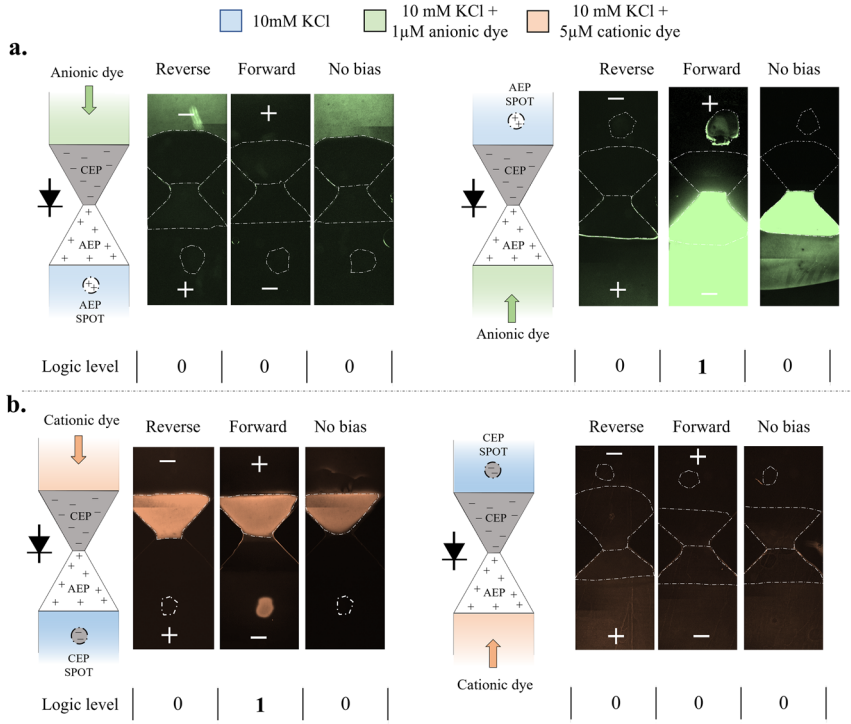

Fig. 3 Single-diode gating of low-abundance molecules: experimental observations. The microfluidic system consisted of the bipolar diode, in addition to an anion-/cation-exchange polyelectrolyte (AEP/CEP) spot to adsorb and accumulate molecules that crossed the diode. Gating was performed for (a) 1 μM anionic dye Alexa Fluor 488 with an AEP spot, and (b) 5 μM cationic dye Atto Rho6G with a CEP spot. Each dye was homogeneously mixed within a 10 mM KCl electrolyte solution and initially ($t = 0$ h) introduced to one side of the diode (represented by the green/orange arrow), while an electrolyte solution absent of the fluorescent dye was introduced to the other side (containing the spot). For each operation mode (reverse, forward, and no bias corresponding to −1, +1, and 0 V, respectively), the fluorescence intensity was measured after an overnight operation ($t = 15$ h). Shortening the length of the polyelectrolytes led to a faster response (Fig. S5†). Measurements of low and high fluorescence intensities on the spot were translated to logic levels '0' and '1', respectively.

indication of the successful passage of the target molecules, in the form of a high-intensity spot, was only obtained when two conditions existed simultaneously (Fig. 3). The diode had to be both forward-biased to maintain high ionic fluxes, and have an electrophoretic driving force acting on the fluorescent molecules in the direction of the side that was initially free of these molecules. In all other cases, no fluorescence intensity was observed for the same duration of operation, suggesting that the crossing rate of molecules was significantly lower. This outcome further supports the dominance of electromigration on the transport of molecules over that of possible convective transport stemming from either the charged polyelectrolytes or the surface charge of the microchannels. For example, gating of the anionic dye required its introduction into the microchannel interfacing with the AEP side so that the molecules within the microchannel would face an 'open' diode when driven by the external electric

field through the diode to the CEP side (Fig. 3a). The opposite was true for the cationic dye, which had to be introduced into the microchannel interfacing with the CEP side (Fig. 3b). Translating the intensity level of the spot to logic readouts of '1' (high fluorescence intensity) and '0' (low fluorescence intensity) resulted in a single logic readout case of '1' out of 6 possible cases (see Fig. 3), as explained above. In addition to the spots, intensity changes within the polyelectrolyte region forming the diode itself and at the interconnecting microchannels could be seen for the different activation cases. However, the changes were highly dependent on the type of dye molecule and on the polyelectrolyte, and didn't necessarily exhibit a similar response in terms of the optical readout. While the anionic dye showed depletion and enrichment within the polyelectrolyte region, the cationic dye permanently adsorbed onto the anion-exchange membrane (AEM) on the polyelectrolyte side, with no apparent sensitivity to the applied potential. This difference may have stemmed from differences in molecule properties, such as size, type, valency, and interactions with the polyelectrolyte surface groups.

Adding a polyelectrolyte spot to the numerical model resulted in results qualitatively similar to those of the experiments (Fig. 4). Low-abundance analyte molecules that crossed the diode gradually accumulated at the polyelectrolyte spot over time. The high fluxes when forward-biasing the diode while

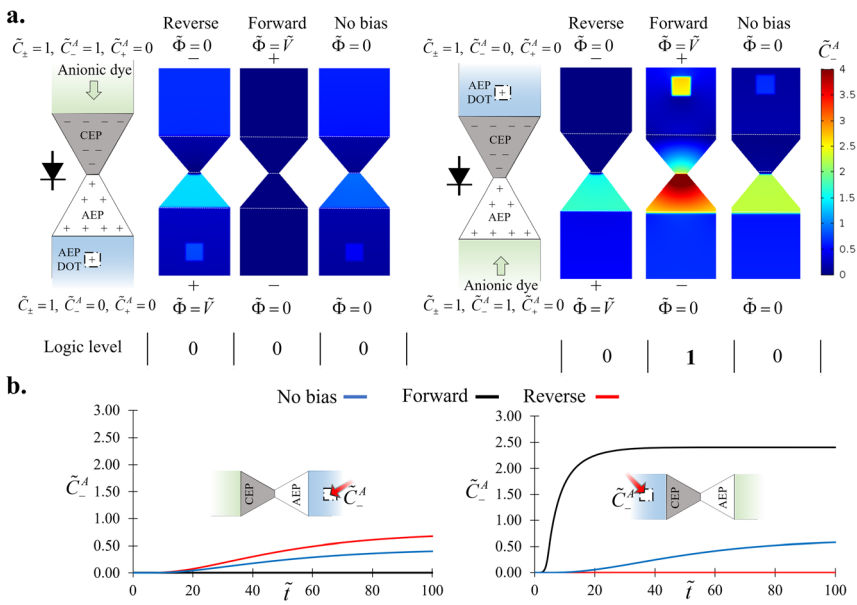

Fig. 4 Numerical investigation of the gating effect of the diode on analyte molecule crossover. (a) The steady-state analyte concentration distribution with varying electric field polarity. The anionic analyte was introduced into either the CEP side (top microchannel) or the AEP side (bottom microchannel). The steady-state analyte concentration at the polyelectrolyte spot was translated to either logic level '1' ($\tilde{C}_-^A > 1$) or '0' ($\tilde{C}_-^A < 1$). (b) The average analyte concentration at the polyelectrolyte spot (marked with a red arrow) plotted as a function of time. The analyte concentration at the polyelectrolyte spot only reached values above 1 when the diode was 'open' and the analyte was simultaneously electrophoretically driven towards the diode.

simultaneously introducing an anionic dye at the AEP-side yielded a larger crossover of the analyte. This crossover was expressed by the enhanced analyte accumulation factor and rate at the polyelectrolyte spot.

Diode-based OR logic gating of low-abundance molecules

Inspired by electronic diode-based logics, multiple diodes were integrated to construct a basic Boolean function of an ionic OR logic gate (Fig. 5). Unlike electric circuits where the logic operation is only performed on the electrical voltage readout level, the ionic circuit also exhibited such functionality in the molecule gating. Low (0) and high (1) logic input levels were realized by directly

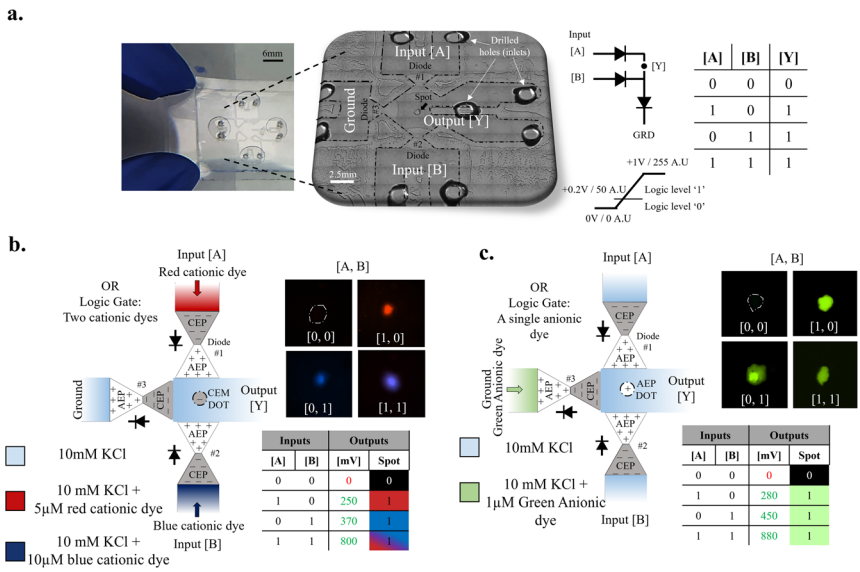

Fig. 5 Diode-based OR logic gating of low-abundance molecules. (a) Left to right: an image of the device, a zoomed-in image of the microfluidic channels taken under a microscope, and a schematic of the electrical circuit, along with a truth table of the OR gate. The ionic OR logic gate contained three diodes (#1, #2 and #3) with two inputs [*A*] and [*B*] of 0 V or +1 V, corresponding to a low ('0') or high ('1') logic input, and an output readout region ([*Y*]). The polyelectrolyte spot at the readout region (*i.e.*, the central microchannel in between all three diodes) was made of either a cation- or anion-exchange polyelectrolyte (CEP or AEP, respectively). A threshold voltage of +0.2 V (voltage range 0 V to +1 V) and a fluorescence intensity of 50 AU (intensity range 0–255 AU) were defined to distinguish between low (below the threshold, '0') and high (above the threshold, '1') logic outputs. (b) An OR logic gate with fluorescently tagged cationic dyes introduced into the input reservoirs. 5 μM Atto Rho 6G (red) and 10 μM Atto 465 (blue) were introduced into inlets [*A*] and [*B*], respectively. The captured fluorescence of the CEP spot after a 12 h operation and its associated color (relative to the emission wavelength) for each input sequence ([*A*,*B*] = [0,0], [1,0], [0,1] or [1,1]) are presented. The electrical and optical output readouts (voltage rounded up to the nearest tenth) with their associated logic levels are summarized in the truth table. (c) An OR logic gate with a fluorescently tagged anionic dye. 1 μM Alexa Fluor 488 (green) was introduced into the inlet reservoir of diode #3. An AEP spot was used as the indicator for the optical logic levels. The intensities measured at the spot after a 15 h operation and the corresponding truth table are presented.

applying 0 V (= ground) and +1 V, respectively. Output readouts were associated with their logic levels based on either the measured potential or fluorescence intensity. A low (0) logic output level was defined for potentials below +0.2 V and fluorescence intensity below 50 AU, while higher values were defined as a high (1) output level. Each input of the OR logic gate (inputs [*A*] or [*B*]) was connected through a diode (diode #1 or #2, respectively) to a shared interconnecting microchannel containing a polyelectrolyte spot where the output readout of the circuit (output [*Y*]) was obtained. If one or both inputs were at logic level '1', a current crossed through the corresponding forward-biased diodes to the shared central microchannel, towards a constantly grounded diode (diode #3) that was forward-biased as well. This, in turn, caused both a voltage drop and molecule transfer across the diodes, resulting in a logic output of '1', as shown in Fig. 5b and c. Logic output '0' was only obtained when both inputs were low with no electrical current passing through the circuit. For example, introduction of cationic dye Atto Rho 6G (shown in red) to the reservoir of input [*A*] and Atto 465 (shown in blue) to the reservoir of input [*B*] resulted in successful gating, in accordance with the input states (Fig. 5b). The CEP spot became highly fluorescent (output logic '1') with red, blue, or purple (mixture of red and blue) signals when the input [*A*,*B*] states were [1,0], [0,1], and [1,1], respectively. No fluorescence was detected (output logic '0') for the input state [0,0]. In agreement with the fluorescence signals of the polyelectrolyte spots, the output voltage associated with logic '1' varied between +250 mV and +800 mV, depending on which and how many inputs were set to high, while logic '0' was associated with 0 mV output when both inputs were set to low (*i.e.*, [0,0]). In contrast to the optical readouts that required operation of several hours to transfer sufficient fluorescently tagged molecules across the diodes, the electrical readouts stabilized much faster (∼a few minutes) as the electrolyte ions only had to be depleted from or enriched at the junction of the diode. Note that each state of the OR logic gate (total 2^2 states) was examined on a different device due to the inability to release the adsorbed molecule from the polyelectrolytes and to restart the gate at the initial conditions of negligible fluorescence intensity (<50 AU) at the polyelectrolyte spot. Thus, geometric variations between the diodes resulted in deviations of the voltage drop across the circuit between states that should have provided a similar output voltage (*e.g.*, [1,0] and [1,0]). Replacing the cationic dyes with an anionic dye (Alexa Fluor 488, shown in green), resulted in a similar gate behavior (Fig. 5c). However, the anionic dye had to be introduced to the reservoir connected to diode #3 to maintain the conditions required for efficient molecule crossover, as found in the previous section. Only when at least one input was set to a high value did the AEP spot at the center become highly fluorescent. These results are in qualitative agreement with those obtained using numerical simulations (Fig. S6†).

Conclusions and outlook

In this work, we presented the use of a bipolar polyelectrolyte-based diode as a logic gate of low-abundance molecule crossover. In activation modes of ±1 V, the diodes exhibited an average current rectification ratio of ∼10 between the steady-state forward- and reverse-biased electric currents, respectively. This current rectification was associated with the ratio of the ion fluxes through the nonideal selective polyelectrolytes that formed the diode, as more ions crossed

the diode under a forward bias. Exploiting the regulation of the ionic fluxes, we experimentally demonstrated, and confirmed by numerical simulations, the crossover of charged, fluorescently tagged low-abundance dye molecules from one side of the diode to the other side. Optical visualizations of the fluorescence intensity were used to estimate the concentrations of the target analytes. The analysis demonstrated that the crossover was only successful when the diode was forward-biased and the target molecules experienced an electrophoretic driving force towards the opposite side of the diode. In all other cases, a significantly lower transport rate was obtained, which can effectively be considered as an absence of crossover. We noted that effects such as chemical interaction of the molecules with the polyelectrolyte surface groups, adsorption, and steric hindrance, in addition to variations in target molecule properties, such as size, type, and valency, can impair the effectiveness of the regulation over the crossover. Inspired by electronic diode-based logics, the single-diode system was extended to multiple-diode ionic circuits that formed a Boolean function of an ionic OR logic gate. The logic operation was performed on the electrical potential and the molecule gating, exploiting the unique advantage of various charge carriers in the ionic environment. This enabled simultaneous classification of both the electrical and optical readouts to discrete logic levels of high ('1') and low ('0'). Yet, when considering more complex computational processes, the number of diode-based logic gates that can be integrated is severely limited due to the degradation of the electrical potential signal and leakage currents associated with each sequential logic gate.[42] To extend the functionality and integration level of ionic circuits, future iontronic circuits should also incorporate ion-based transistors into the circuit in order to compensate for voltage drops. Such a future direction in iontronic circuits, which has tremendous potential in terms of functionality and integration level, is reminiscent of the technological revolution that integrated electronic circuits have undergone since the invention of the solid-state transistor.[49]

Conflicts of interest

There are no conflicts to declare.

Acknowledgements

This work was supported by the Israel Science Foundation (ISF 1934/20) and the Israel Innovation Authority (IIA). We are grateful to the Tel-Aviv University Center for Nanoscience and Nanotechnology for their support in the fabrication of the microfluidic chips. We thank Prof. Alex Fish and Noa Edri Fraiman from Bar-Ilan University for the fruitful discussions.

References

1 R. Plonsey and R. C. Barr, *Bioelectricity. A Quantitative Approach*, Springer, 3rd edn, 2007.
2 T. Arbring Sjöström, M. Berggren, E. O. Gabrielsson, P. Janson, D. J. Poxson, M. Seitanidou and D. T. Simon, A Decade of Iontronic Delivery Devices, *Adv. Mater. Technol.*, 2018, **3**(5), 1700360.

3 H. Chun and T. D. Chung, Iontronics, *Annu. Rev. Anal. Chem.*, 2015, **8**, 441–462, DOI: **10.1146/annurev-anchem-071114-040202**.
4 S. Zulkarnaen Bisri, S. Shimizu, M. Nakano and Y. Iwasa, Endeavor of Iontronics: From Fundamentals to Applications of Ion-Controlled Electronics, *Adv. Mater.*, 2017, **29**, 1607054, DOI: **10.1002/adma.201607054**.
5 Y. Chang, L. Wang, R. Li, Z. Zhang, Q. Wang, J. Yang, C. F. Guo and T. Pan, First Decade of Interfacial Iontronic Sensing: From Droplet Sensors to Artificial Skins, *Adv. Mater.*, 2021, **33**(7), 2003464, DOI: **10.1002/adma.202003464**.
6 L. Sen, P. Ning, Z. Zijie, L. Ruya, L. Baoqing, C. Jiaru, L. Guanglin, C. Yu and P. Tingrui, All-in-One Iontronic Sensing Paper Sen, *Adv. Funct. Mater.*, 2019, **29**, 1807343.
7 Y. Hou and X. Hou, Bioinspired Nanofluidic Iontronics, *Science*, 2021, **373**(6555), 628–629, DOI: **10.1126/science.abj0437**.
8 A. Piruska, M. Gong, J. V. Sweedler and P. W. Bohn, Nanofluidics in Chemical Analysis, *Chem. Soc. Rev.*, 2010, **39**, 1060–1072, DOI: **10.1039/b900409m**.
9 D. G. Haywood, A. Saha-Shah, L. A. Baker and S. C. Jacobson, Fundamental Studies of Nanofluidics: Nanopores, Nanochannels, and Nanopipets, *Anal. Chem.*, 2015, **87**(1), 172–187, DOI: **10.1021/ac504180h**.
10 K. Xiao, L. Jiang and M. Antonietti, Ion Transport in Nanofluidic Devices for Energy Harvesting, *Joule*, 2019, **3**(10), 2364–2380, DOI: **10.1016/j.joule.2019.09.005**.
11 Z. Zhang, L. Wen and L. Jiang, Nanofluidics for Osmotic Energy Conversion, *Nat. Rev. Mater.*, 2021, **6**(7), 622–639, DOI: **10.1038/s41578-021-00300-4**.
12 S. K. Das, M. D. Austin, M. C. Akana, P. Deshpande, H. Cao and M. Xiao, Single Molecule Linear Analysis of DNA in Nano-Channel Labeled with Sequence Specific Fluorescent Probes, *Nucleic Acids Res.*, 2010, **38**(18), e177, DOI: **10.1093/nar/gkq673**.
13 B. N. Miles, A. P. Ivanov, K. A. Wilson, F. Dogan, D. Japrung and J. B. Edel, Single Molecule Sensing with Solid-State Nanopores: Novel Materials, Methods, and Applications, *Chem. Soc. Rev.*, 2013, **42**(1), 15–28, DOI: **10.1039/c2cs35286a**.
14 S. J. Kim, Y. A. Song and J. Han, Nanofluidic Concentration Devices for Biomolecules Utilizing Ion Concentration Polarization: Theory, Fabrication, and Applications, *Chem. Soc. Rev.*, 2010, **39**(3), 912–922, DOI: **10.1039/b822556g**.
15 B. Sabbagh, E. Stolovicki, S. Park, D. A. Weitz and G. Yossifon, Tunable Nanochannels Connected in Series for Dynamic Control of Multiple Concentration-Polarization Layers and Preconcentrated Molecule Plugs, *Nano Lett.*, 2020, **20**, 8524–8533, DOI: **10.1021/acs.nanolett.0c02973**.
16 D. Stein, M. Kruithof and C. Dekker, Surface-Charge-Governed Ion Transport in Nanofluidic Channels, *Phys. Rev. Lett.*, 2004, **93**(3), 035901, DOI: **10.1103/PhysRevLett.93.035901**.
17 A. Plecis, R. B. Schoch and P. Renaud, Ionic Transport Phenomena in Nanofluidics: Experimental and Theoretical Study of the Exclusion-Enrichment Effect on a Chip, *Nano Lett.*, 2005, **5**(6), 1147–1155, DOI: **10.1021/nl050265h**.
18 T. Luo, S. Abdu and M. Wessling, Selectivity of Ion Exchange Membranes: A Review, *J. Membr. Sci.*, 2018, **555**, 429–454, DOI: **10.1016/j.memsci.2018.03.051**.
19 T. Sata, Studies on Anion Exchange Membranes Having Permselectivity for Specific Anions in Electrodialysis — Effect of Hydrophilicity of Anion

Exchange Membranes on Permselectivity of Anions, *J. Membr. Sci.*, 2000, **167**, 1–31.

20 H. Miyoshi, Diffusion Coefficients of Ions through Ion Exchange Membrane in Donnan Dialysis Using Ions of Different Valence, *J. Membr. Sci.*, 1998, **141**(1), 101–110, DOI: **10.1016/S0376-7388(97)00297-4**.

21 T. Okada, G. Xie, O. Gorseth, S. Kjelstrup, N. Nakamura and T. Arimura, Ion and Water Transport Characteristics of Nafion Membranes as Electrolytes, *Electrochim. Acta*, 1998, **43**(24), 3741–3747, DOI: **10.1016/S0013-4686(98)00132-7**.

22 T. Arbring Sjöström, A. Jonsson, E. Gabrielsson, L. Kergoat, K. Tybrandt, M. Berggren and D. T. Simon, Cross-Linked Polyelectrolyte for Improved Selectivity and Processability of Iontronic Systems, *ACS Appl. Mater. Interfaces*, 2017, **9**(36), 30247–30252, DOI: **10.1021/acsami.7b05949**.

23 Q. Zhao, Q. F. An, Y. Ji, J. Qian and C. Gao, Polyelectrolyte Complex Membranes for Pervaporation, Nanofiltration and Fuel Cell Applications, *J. Membr. Sci.*, 2011, **379**(1–2), 19–45, DOI: **10.1016/j.memsci.2011.06.016**.

24 T. Boudou, T. Crouzier, K. Ren, G. Blin and C. Picart, Multiple Functionalities of Polyelectrolyte Multilayer Films: New Biomedical Applications, *Adv. Mater.*, 2010, **22**(4), 441–467, DOI: **10.1002/adma.200901327**.

25 W. Zhang, Q. Zhao and J. Yuan, Porous Polyelectrolytes: The Interplay of Charge and Pores for New Functionalities, *Angew. Chem., Int. Ed.*, 2018, **57**(23), 6754–6773, DOI: **10.1002/anie.201710272**.

26 S. H. Han, S. Il Kim, H. R. Lee, S. M. Lim, S. Y. Yeon, M. A. Oh, S. Lee, J. Y. Sun, Y. C. Joo and T. D. Chung, Hydrogel-Based Iontronics on a Polydimethylsiloxane Microchip, *ACS Appl. Mater. Interfaces*, 2021, **13**(5), 6606–6614, DOI: **10.1021/acsami.0c19892**.

27 J. H. Han, K. B. Kim, H. C. Kim and T. D. Chung, Ionic Circuits Based on Polyelectrolyte Diodes on a Microchip, *Angew. Chem., Int. Ed.*, 2009, **48**(21), 3830–3833, DOI: **10.1002/anie.200900045**.

28 J. H. Han, K. B. Kim, J. H. Bae, B. J. Kim, C. M. Kang, H. C. Kim and T. D. Chung, Ion Flow Crossing over a Polyelectrolyte Diode on a Microfluidic Chip, *Small*, 2011, **7**(18), 2629–2639, DOI: **10.1002/SMLL.201100827**.

29 O. J. Cayre, T. C. Suk and O. D. Velev, Polyelectrolyte Diode: Nonlinear Current Response of a Junction between Aqueous Ionic Gels, *J. Am. Chem. Soc.*, 2007, **129**(35), 10801–10806, DOI: **10.1021/ja072449z**.

30 K. Nyamayaro, V. Triandafilidi, P. Keyvani, J. Rottler, P. Mehrkhodavandi and S. G. Hatzikiriakos, The Rectification Mechanism in Polyelectrolyte Gel Diodes, *Phys. Fluids*, 2021, **33**(3), 032010.

31 Y. Zhao, S. Dai, Y. Chu, X. Wu and J. Huang, A Flexible Ionic Synaptic Device and Diode-Based Aqueous Ion Sensor Utilizing Asymmetric Polyelectrolyte Distribution, *Chem. Commun.*, 2018, **54**(59), 8186–8189, DOI: **10.1039/c8cc04539a**.

32 Y. Wang, Z. Wang, Z. Su and S. Cai, Stretchable and Transparent Ionic Diode and Logic Gates, *Extreme Mech. Lett.*, 2019, **28**, 81–86, DOI: **10.1016/j.eml.2019.03.001**.

33 T. Teorell, An Attempt to Formulate a Quantitative Theory of Membrane Permeability, *Proc. Soc. Exp. Biol. Med.*, 1935, **33**(2), 282–285.

34 R. E. Moussaoui, G. Pourcelly, M. Maeck, H. D. Hurwitz and C. Gavach, Co-Ion Leakage through Bipolar Membranes Influence on I-V Responses and Water-Splitting Efficiency, *J. Membr. Sci.*, 1994, **90**(3), 283–292, DOI: **10.1016/0376-7388(94)80078-2**.

35 M. A. Blommaert, J. A. H. Verdonk, H. C. B. Blommaert, W. A. Smith and D. A. Vermaas, Reduced Ion Crossover in Bipolar Membrane Electrolysis *via* Increased Current Density, Molecular Size, and Valence, *ACS Appl. Energy Mater.*, 2020, **3**(6), 5804–5812, DOI: **10.1021/acsaem.0c00687**.

36 I. Vlassiouk, S. Smimov and Z. Siwy, Nanofluidic Ionic Diodes. Comparison of Analytical and Numerical Solutions, *ACS Nano*, 2008, **2**(8), 1589–1602, DOI: **10.1021/nn800306u**.

37 R. Peng, Y. Pan, B. Liu, Z. Li, P. Pan, S. Zhang, Z. Qin, A. R. Wheeler, X. Tang and X. Liu, Understanding Carbon Nanotube-Based Ionic Diodes Design and Mechanism, *Small*, 2021, **17**, 2100383.

38 M. Ali, P. Ramirez, S. Nasir, J. Cervera, S. Mafe and W. Ensinger, Ionic Circuitry with Nanofluidic Diodes, *Soft Matter*, 2019, **15**, 9682, DOI: **10.1039/c9sm01654f**.

39 Y. Wang, Z. Wang, Z. Su and S. Cai, Stretchable and Transparent Ionic Diode and Logic Gates, *Extreme Mech. Lett.*, 2019, **28**, 81–86, DOI: **10.1016/j.eml.2019.03.001**.

40 Q. Dong, J. Jiang, Y. Wang and J. Zhai, Geometric Tailoring of Macroscale Ti3C2TxMXene Lamellar Membrane for Logic Gate Circuits, *ACS Nano*, 2021, **15**, 19266–19274, DOI: **10.1021/acsnano.1c05170**.

41 M. Ali, S. Mafe, P. Ramirez, R. Neumann and W. Ensinger, Logic Gates Using Nanofluidic Diodes Based on Conical Nanopores Functionalized with Polyprotic Acid Chains, *Langmuir*, 2009, **25**(20), 11993–11997, DOI: **10.1021/la902792f**.

42 B. Sabbagh, N. E. Fraiman, A. Fish and G. Yossifon, Designing with Iontronic Logic Gates: From a Single Polyelectrolyte Diode to an Integrated Ionic Circuit, *ACS Appl. Mater. Interfaces*, 2023, **15**(19), 23361–23370, DOI: **10.1021/acsami.3c00062**.

43 T. Trorell, An Attempt to Formulate a Quantitative Theory of Membrane Permeability, *Proc. Soc. Exp. Biol. Med.*, 1935, **33**(2), 282–285.

44 J. A. Manzanares, W. D. Murphy, S. Mafe and H. Reiss, Numerical Simulation of the Nonequilibrium Diffuse Double Layer in Ion-Exchange Membranes, *J. Phys. Chem.*, 1993, **97**(32), 8524–8530, DOI: **10.1021/j100134a023**.

45 L. J. Cheng and H. C. Chang, Microscale PH Regulation by Splitting Water, *Biomicrofluidics*, 2011, **5**(4), 046502.

46 R. Simons, Water Splitting in Ion Exchange Membranes, *Electrochim. Acta*, 1985, **30**(3), 275–282.

47 R. Pärnamäe, S. Mareev, V. Nikonenko, S. Melnikov, N. Sheldeshov, V. Zabolotskii, H. V. M. Hamelers and M. Tedesco, Bipolar Membranes: A Review on Principles, Latest Developments, and Applications, *J. Membr. Sci.*, 2021, **617**, 118538, DOI: **10.1016/j.memsci.2020.118538**.

48 R. Abu-Rjal and Y. Green, Bipolar Nanochannels: A Systematic Approach to Asymmetric Problems, *ACS Appl. Mater. Interfaces*, 2021, **13**(23), 27622–27634, DOI: **10.1021/acsami.1c05643**.

49 H. Tigelaar *How Transistor Area Shrank by 1 Million Fold*; Springer, 2020. DOI: **10.1007/978-3-030-40021-7**.